

Hole Defects and Nitrogen Doping in Graphene: Implication for Supercapacitor Applications

Gaixia Luo,^{†,‡} Lizhao Liu,[†] Junfeng Zhang,[†] Guobao Li,[†] Baolin Wang,[‡] and Jijun Zhao^{*,†,§}

[†]Key Laboratory of Materials Modification by Laser, Ion and Electron Beams, Ministry of Education, Dalian University of Technology, Dalian 116024, China

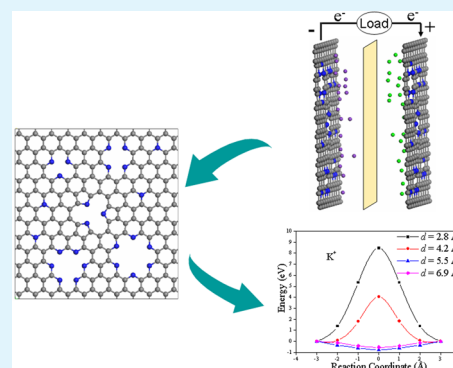
[‡]Key Laboratory for Advanced Technology in Environmental Protection of Jiangsu Province, Yancheng Institute of Technology, Jiangsu, 224051, China

[§]Yangzhou Institute of Energy and Material, Chinese Academy of Sciences, Yangzhou 225127, China

S Supporting Information

ABSTRACT: One great challenge for supercapacitor is to achieve high energy capacity and fast charge/discharge rates simultaneously. Porous graphene with large surface area is a promising candidate for electrode materials of supercapacitor. Using first-principles calculations and non-equilibrium Green's function technique, we have explored the formation energies, mechanical properties, diffusion behaviors and electrical conductance of graphene sheets with various hole defects and/or nitrogen doping. Interestingly, graphene sheets with pyridinic-like holes (especially hexagonal holes) can be more easily doped with nitrogen and still retain the excellent mechanical properties of pristine graphene that is beneficial for the long cycle life. Porous graphene electrode with moderate hole diameter of 4.2–10 Å facilitates efficient access of electrolyte and exhibit excellent rate capability. In addition, doping with nitrogen as electron donors or proton attractors leads to charge accumulation and generates higher pseudocapacitance. Transmission coefficients of N-doped graphene sheets with pyridinic-like holes are only moderately reduced with regard to that of pristine graphene and are insensitive to the detailed geometry parameters. Overall, N-doped graphene with pyridinic-like holes exhibits exciting potentials for high performance energy storage in supercapacitor devices.

KEYWORDS: supercapacitors, graphene, hole, doping



1. INTRODUCTION

Supercapacitors (also known as ultracapacitors or electrochemical capacitors) are extensively investigated as possible auxiliary energy storage devices used with rechargeable batteries. Supercapacitors store energy through electrochemical charge accumulation or Faradaic reaction at the electrode/electrolyte interface. Compared with conventional batteries, supercapacitors are superior for their higher power density and simple charging circuit, but suffer from very low energy density (e.g., 5 Wh/kg_{cell} for commercial activated carbon-based supercapacitors compared to 100–150 Wh/kg_{cell} for commercial Li-ion battery¹). Therefore, searching for appropriate electrode materials for supercapacitors is the key to achieving high capacitance. So far, carbon-based electrodes such as activated carbons,² ordered mesoporous carbons,³ and carbon nanotubes,⁴ have been widely used in the supercapacitor industry owing to their high surface area and good electrical conductivity.⁵ However, their supercapacitor capacitances are still not sufficient for many applications.

As a superstar material in the past decade, graphene is also regarded as an attractive candidate for electrode materials of supercapacitors because of its high electrical conductivity and

large theoretical surface area (2630 m²/g).^{6,7} However, the specific area of actual graphene materials is reduced by agglomeration or even re-stacking of the graphene sheets. Cheng et al.⁸ fabricated graphene/carbon nanotube (CNT) electrode for supercapacitors and found that the presence of CNT in the composite prevented graphene from restacking. After oxidizing the graphene sheet, the epoxide and hydroxyl groups could expand the interlayer van der Waals (vdW) distance to 7 Å.^{9,10} In spite of the high theoretical value of 550 F/g, low actual capacitance of graphene (130 and 99 F/g in aqueous and organic electrolyte, respectively) dissatisfies the demand of commercial applications.¹¹ The efficiency of surface area can be improved by introducing pores into graphene sheet.¹² It was found that supercapacitors with porous graphene yielded a high capacitance of 200 F/g at a current density of 0.7 A/g.¹³ Therefore, the current challenge is to develop graphene materials tailoring with adequate hole size distribution in order to achieve optimal capacitance.¹⁴

Received: August 15, 2013

Accepted: October 17, 2013

Published: October 17, 2013

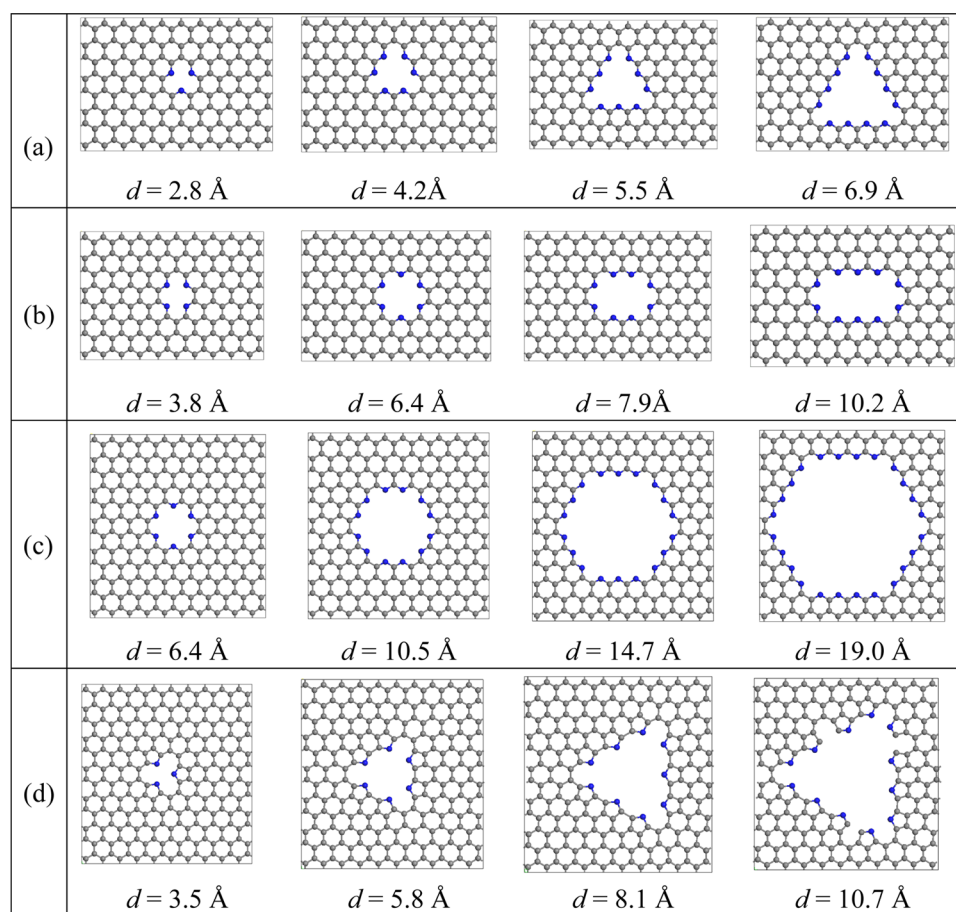


Figure 1. Structural models with holes of different shapes and sizes: (a) triangular, (b) rectangular, and (c) hexagonal holes for pyridinic-like; (d) pyrrolic-like. Gray sphere, carbon; blue sphere, carbon with the dangling bond or nitrogen.

In addition to the pristine graphene materials, there have been some recent efforts devoted to further improving the electrocatalytic activity via nitrogen doping of graphene with pseudocapacitive effect and accessible porosity.^{15–18} For example, Jeong et al.¹⁵ developed N-doped graphene via plasma process for high performance ultracapacitors, whose capacitances (~ 280 F/g) were about four times larger than those of the pristine graphene (~ 70 F/g) in aqueous electrolytes. As reported by Qiu et al.,¹⁶ N-doped graphene-based supercapacitor delivers remarkable energy and power when operated at higher voltage (up to 4 V). Sun and coworkers¹⁹ showed that nitrogen-doped graphene with high nitrogen level exhibits excellent capacitive behavior (326 F/g, 0.2 A/g), superior cycling stability and Coulombic efficiency (99.58 %) after 2000 cycles.

Until now, several approaches such as chemical vapor deposition (CVD),²⁰ arc discharge,²¹ thermal annealing,²² and nitrogen plasma process¹⁵ have been employed to synthesize nitrogen-doped graphene materials. According to X-ray photoelectron spectroscopy (XPS),¹⁷ there are generally three types of nitrogen dopants: (i) pyridinic-like N connecting with two carbon atoms and donating one p electron to the aromatic π system, (ii) pyrrolic-like N connecting with two carbon atoms and contributing two π electrons to the π system, (iii) quaternary-like (graphitic-like) N substituting one carbon atom within the graphene lattice. Experimentally, the specific bonding types of nitrogen can be controlled in the synthesis process.¹⁹ Most importantly, N doping is able to introduce

holes on graphene sheets that facilitate electrolyte penetration and ion transport.²³

Parallel to experiments, theoretical studies revealed that N doping can effectively tailor the electronic property and chemical reactivity of graphene.^{24–28} For instance, N dopants in graphene as electron donor result into band shift to accommodate extra electrons.²⁴ Comparison of electronic structures of N-doped graphene, including graphitic, pyridinic and pyrrolic nitrogens, showed that the pyridinic graphene has strongest electron deficiency for accepting electrons.²⁵ Theoretical efforts have also been devoted to understanding the fundamental properties and electrochemical behavior of N-doped graphene electrode materials for batteries.^{29–31} Yan and co-workers²⁹ investigated O₂ adsorption and dissociation on the surface of pristine and N-doped graphene as electrode for Li-air batteries, suggesting that N-doped graphene can serve as catalyst for O₂ dissociation reaction. Wu et al.³⁰ investigated Li adsorption, diffusion, and desorption in pristine, B- or N-doped graphene. Among them, N-doped quaternary-like graphene exhibited lower diffusion and desorption barrier; thus it is a promising anode material with high-rate charge/discharge ability for Li-ion batteries. Ma et al.³¹ predicted that pyridinic graphene is most suitable for Li storage with reversible capacity reaching 1262 mAh/g, which is higher than the experimental result of 1043 mAh/g.³² That is to say, graphene materials with pyridinic defects synthesized in experiments would be more appropriate as anode for Li battery.

Despite the aforementioned progresses, there are still many unclear issues about the nitrogen-doped graphene as electrode material for supercapacitors. For example, will these hole defects degrade the thermodynamic stability and electrical conductance of the graphene electrode? Will graphene sheets with various holes still retain their excellent mechanical strength? What is the optimal shape and size of holes for ion diffusion? Which kind of C–N bonding configuration is responsible for the enhanced electrocatalytic activity of N-doped graphene? Certainly, a thorough theoretical investigation at atomistic scale is imperative for optimizing the microstructures of graphene-based electrode materials and improving the performance of supercapacitors.

To shed some light on these critical issues for the graphene-based electrode materials of supercapacitors, here we carried out density functional theory (DFT) computations on the thermodynamic stabilities, mechanical properties, diffusion behavior and transport properties of undoped and N-doped graphene with different geometries of holes, aiming to enhance the performance of supercapacitors by appropriate incorporation of holes. Compared to the undoped graphene, N-doped graphene with pyridinic-like holes (especially hexagonal holes) are thermodynamically more stable and retain their excellent mechanical properties. Within the optimal diameter (4.2 Å to 10 Å), the N-doped graphene sheets with pyridinic-like hexagonal hole not only allow fast diffusion rate for electrolyte ions but also possess preferable electron transmission property.

2. STRUCTURAL MODELS

Starting from a perfect graphene sheet, we introduced the pyridinic-like and pyrrolic-like nitrogen dopants as previously observed in XPS experiments¹⁷ to explore hole effect. In the case of pyridinic-like doping, three series of holes in different shapes (i.e., triangle, rectangle, and hexagon) have been considered to investigate the hole shape effect. For comparison, we considered undoped graphene sheets with same shape of holes. Here hole diameter (d) is defined as incircle diameter for the hexagonal and triangular holes, and diagonal length for the rectangular holes, respectively.

We adopted two kinds of simulation supercells for graphene sheets: (i) 160 carbon atoms with dimensions of 24.6 Å × 17.06 Å for the pyridinic-like holes with triangular and rectangular shapes; (ii) 240 carbon atoms with dimensions of 24.6 Å × 25.59 Å for the pyridinic-like holes of hexagonal shape and the pyrrolic-like holes of triangular shape. On the periphery of holes, the carbon atoms with dangling bonds were substituted by nitrogen to further construct N-doped graphene sheets (see Figure 1), whereas all edge dangling bonds are not passivated for undoped graphene for a direct comparison. It is known that a graphene lattice has two sets of sublattices. Our test calculations show that creating hole or substituting N on different sublattice atoms has a negligible effect on the computational results of relevant physical properties such as edge formation energy.

3. COMPUTATIONAL METHODS

All first-principles calculations were performed using the spin-polarized density functional theory with the projector-augmented wave (PAW) method,^{33,34} as implemented in the Vienna Ab initio Simulation Package (VASP).^{33,35} The Perdew–Burke–Ernzerhof (PBE) functional within the generalized gradient approximation (GGA) was employed to describe the exchange–correlation interaction.³⁶ The valence electron states were expanded in a plane wave basis with kinetic

energy cutoff of 380 eV. The $2 \times 3 \times 1$ and $2 \times 2 \times 1$ Monkhorst–Pack k grids were used for sampling the Brillouin zones of the 24.6 Å × 17.06 Å and 24.6 Å × 25.59 Å supercells, respectively. To avoid interaction between adjacent graphene layers, each graphene sheet was separated by 12 Å of vacuum. The convergence criteria of structural optimization were chosen as maximum force on each atom less than 0.02 eV/Å and energy change less than 1×10^{-4} eV. Our test calculations showed that further increasing cutoff energy or k grid only leads to little changes on the computational results.

Taking KCl as a representative electrolyte,^{37,38} we simulated the diffusion behaviors of K^+ and Cl^- ions. The positive (negative) charged ion was modeled by removing (adding) one electron from the simulation supercell. Bader analysis³⁹ demonstrated that this positive (negative) charge mainly resides on the K^+ (Cl^-) ion. The climbing-image nudged elastic band (CI-NEB) method⁴⁰ was used to search saddle points and determine the minimum energy path during the diffusion path of K^+ and Cl^- ions through different holes by minimization of a set of intermediate images between two known configurations. The spring constant between adjacent images was set as 5.0 eV Å⁻¹. Each path was interpolated by fitting a cubic polynomial through all images, guided by the force tangent to the reaction coordinate.

The electrical transmission coefficients of undoped and N-doped graphene sheets with inclusion of different holes were calculated using the Keldysh non-equilibrium Green's function (NEGF) formalism implemented in the Nanodcal code.^{41,42} The transport boundary conditions were treated by real-space numerical procedures. The quantum transmission was calculated by including self-energies for coupling of a 2 nm wide scattering region with one hole inside graphene sheet along the direction of electrodes under zero bias voltage. Along the direction of electrodes, the scattering region is finite while the left and right electrode regions are periodic. Both left/right electrodes are modeled by 24-atom cell of graphene sheet with dimension of 12.79 Å × 4.93 Å (see Figure S1 in the Supporting Information).

4. RESULTS AND DISCUSSION

4.1. Formation Energies of Hole Edge. Thermodynamic stability is a crucial factor for an electrode material of supercapacitors, especially for the graphene sheet with certain amount of holes. Since the hole periphery can be regarded as crimping edges into a loop, we discussed stabilities of the hole edges in terms of formation energies and aimed to elucidate the role of hole and nitrogen doping. Here formation energy per unit length of edge, i.e., edge formation energy (E_F^L , eV/Å), was adopted to describe the thermodynamic stability of hole edge, which can be computed by the following formula

$$E_F^L = \left(E_{C_xN_y} - xE_C - \frac{y}{2}E_{N_2} \right) / L \quad (1)$$

where $E_{C_xN_y}$ is the energy of system with hole, E_C is the energy per C atom in perfect graphene, E_{N_2} is the energy of an isolated N_2 molecule, and y denotes number of N atoms, respectively. By definition, a positive E_F^L means that hole generation is an endothermic process, while a negative value indicates an exothermic one. Therefore, E_F^L can be used to compare thermodynamic stability of the holes of different sizes and shapes inside a graphene sheet.

Figure 2a–c displays E_F^L as a function of hole diameter d for the pyridinic-like holes of different shapes (triangular, rectangular, and hexagonal) in the undoped and N-doped graphene sheets, corresponding to the structural models in Figure 1a–c. To compare the thermodynamic stabilities of different bonding types, E_F^L for pyrrolic-like triangular holes of the undoped and N-doped graphenes are also depicted in

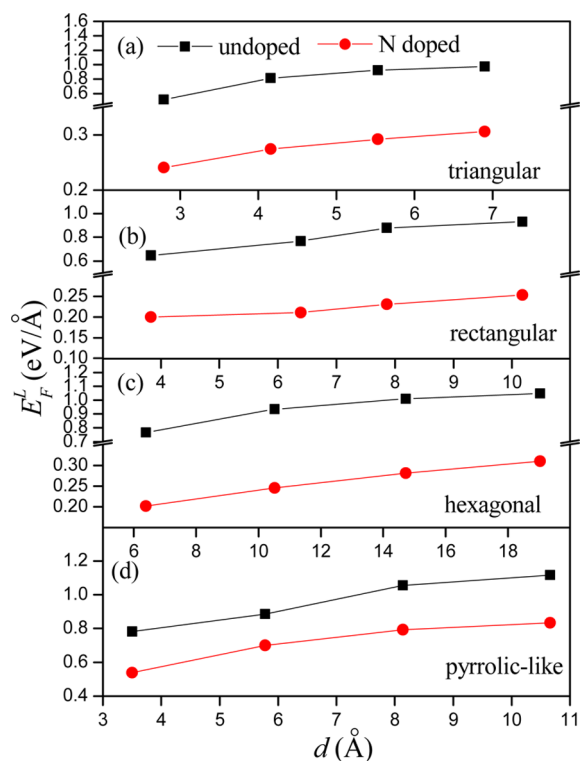


Figure 2. E_F^L as a function of d with different hole shapes: (a) triangular, (b) rectangular, and (c) hexagonal holes for pyridinic-like; and (d) triangular for pyrrolic-like referring to that in the undoped and N-doped graphene sheets.

Figure 2d. For all systems explored, the edge formation energies are positive; thus hole formation in graphene sheet is always endothermic with reduced thermodynamic stability. For every kind of holes, E_F^L increases with d , and then gradually converges to the formation energy of graphene edge. The computed E_F^L for zigzag-edged holes (without nitrogen doping) with large d is close to the formation energy for the zigzag edge of graphene (1.15–1.31 eV) from previous DFT calculations.^{43–45} In addition, E_F^L of the pyrrolic-like hole in undoped graphene is higher than that for the pyridinic-like hole with comparable size, suggesting that formation of a pyrrolic-like hole is less energetically favorable. In short, formation energy of a hole defect depends sensitively on the detailed bonding environment.

Compared to the undoped graphene systems, although hole formation energies for N-doped graphene sheets are still positive, the amplitude of E_F^L is significantly reduced by about 0.2–0.7 eV. In other words, holes on graphene sheet are in favor of N doping. For a 2D graphene sheet with three-coordinated sp^2 hybridization, there are dangling bonds at the hole edge due to unsaturated σ electrons. When a N atom replaces a C atom on the hole edge, two extra p electrons from N atom form a lone pair, which cancels the dangling bonds and partially stabilizes the system.

Instead of hole periphery, we also placed the substitutional N atom in the interior of graphene sheet and computed the corresponding formation energies E_F^N of N dopant as

$$E_F^N = (E_{C_xN_y} - xE_C - y/2E_{N_2})/y \quad (2)$$

The computed E_F^N for N dopant on hole edge and interior site are plotted in Figure S2 in the Supporting Information for

different hole shapes. For all systems considered, nitrogen doping at the hole edge are always energetically more favorable than the interior site by 0.47–0.66 eV, in agreement with previous theoretical report for hydrogenated zigzag graphene nanoribbon (0.59 eV).²⁸ Therefore, the C atoms on hole rim can be more easily substituted by N atoms than the interior C atoms. This is consistent with experimental observations^{12,46} that formation of C–N bond occurred at the edges of graphene sheet where the chemical reactivity is high.

From the above discussions of formation energies, creating different zigzag-edged holes on N doped graphene sheet only costs moderate energy penalty of 0.20–0.31 eV/Å, whereas a formation energy of 0.51–1.05 eV/Å is required for undoped graphene sheet. Therefore, N doping on the pyridinic-like hole in graphene is easier from thermodynamic point of view.

4.2. Diffusion Behavior. Ion diffusion in electrodes is critical in determining the power performance and energy efficiency of supercapacitors.⁴⁷ Obviously, hole size is a key factor affecting the diffusion behavior of ions. For example, Raymundo-Pinero et al.⁴⁸ showed that an adequate hole size is important to achieve high capacitance and found a maximum capacitance for hole sizes of 0.7 nm and 0.8 nm in aqueous and organic electrolytes, respectively. Chmiola et al.⁴⁹ revealed anomalous increase in capacitance of about 13 $\mu\text{F}/\text{cm}^2$ when the hole size is less than the size of solvated ion (~ 1 nm) in an organic electrolyte.

It is well-known that the diffusion constant is mainly determined by the activation barrier,⁵⁰ that is, lower activation energy means faster diffusion rate. Taking K^+ and Cl^- ions as representatives, we calculated their diffusion barriers for penetrating the undoped and doped graphene sheets with different holes towards a better understanding of ion transport in those channels. At the beginning, a K^+ or Cl^- ion was placed far away from the hole with a vertical distance of 3 Å along the center of hole. Then this ion vertically passed through the hole with a step of 0.5 Å until reaching a vertical distance of 3 Å on the other side. The detailed energy profiles along the diffusion paths for every hole are given in Figures S3–S6 of the Supporting Information. To present an overall picture, the diffusion barriers of K^+ and Cl^- ion for the undoped or N-doped graphene are plotted as function of hole size d in Figures 3 and 4, respectively.

From our theoretical results, one can see that the influence of hole shape on activation energy is insignificant and the hole size effect is dominant. No matter the existence of nitrogen dopants, when hole diameter is substantially larger than 10 Å, the energy barriers are close to zero, implying interaction between graphene hole edge and diffusive ion is negligible. Further increasing hole diameter only favors ion penetration very little but certainly degrades the thermodynamic stability and mechanical property of the graphene sheet (which will be discussed later). On the other hand, as hole diameter goes down to ≤ 4.2 Å, which is comparable to ion diameters (3.28 Å for K^+ and 3.62 Å for Cl^-),⁵¹ the energy barrier for ion penetration dramatically increases owing to steric effect. This finding coincides well with previous experimental results by Salitra and co-workers that a hole diameter above 4 Å can be active in electric double layer charging in aqueous solution.⁵²

For the intermediate hole diameters between 4.2 and 10 Å, the amplitudes of energy barriers are usually less than ~ 1 eV for the undoped graphene systems, which means that the ion can overcome the barriers and permeate the hole in a moderate range of operating temperatures. Previously, Beguin et al.

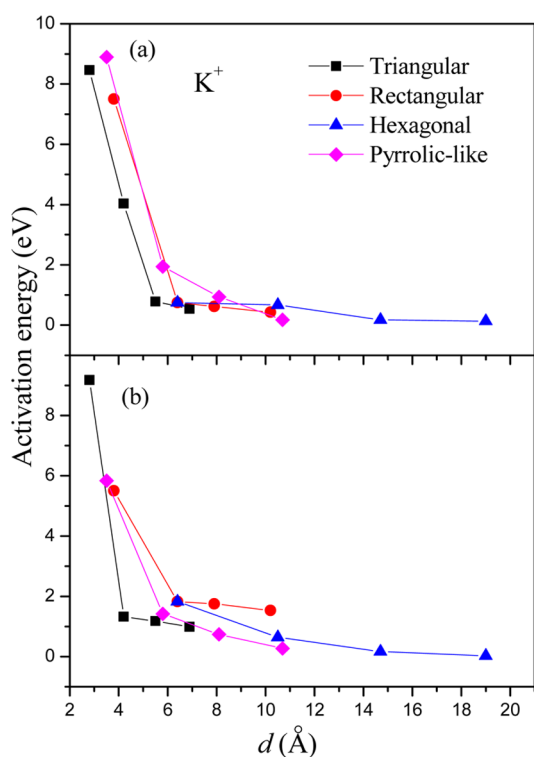


Figure 3. Activation energy for the K^+ ions passing through (a) undoped graphene and (b) N-doped graphene with different hole diameters (d).

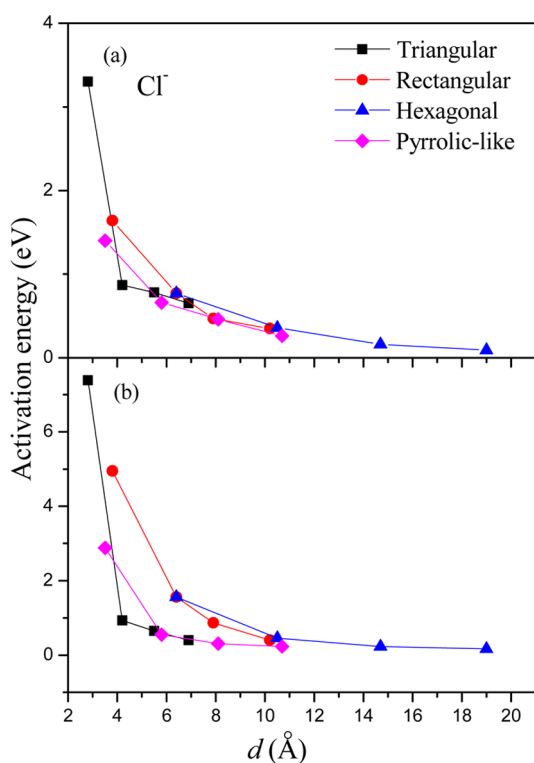


Figure 4. Activation energy for the Cl^- ions passing through (a) undoped graphene and (b) N-doped graphene with different hole diameters (d).

concluded that the optimal hole diameter for EDL capacitance is 7 Å in aqueous media and 8 Å in organic electrolytes, respectively.⁴⁸ In addition, as shown in Table 1 and Figures S3

Table 1. Activation Energies (eV) for the K^+ and Cl^- Ions Passing through the Undoped Graphene and N-Doped Graphene with Different Hole Diameter (d)

	d (Å)	undoped graphene		N-graphene	
		K^+	Cl^-	K^+	Cl^-
triangular	2.8	8.46	3.30	9.18	7.38
	4.2	4.03	0.87	1.33	0.93
	5.5	-0.78	-0.78	-1.18	0.65
	6.9	-0.54	-0.65	-0.99	0.40
rectangular	3.8	7.50	1.64	5.50	4.95
	6.4	-0.75	-0.77	-1.83	1.56
	7.9	-0.62	-0.47	-1.75	0.87
	10.2	-0.43	-0.35	-1.53	0.40
hexagonal	6.4	-0.75	-0.77	-1.83	1.56
	10.5	-0.67	-0.36	-0.64	0.46
	14.7	-0.18	-0.16	-0.17	0.23
	19.0	-0.13	-0.09	-0.03	0.17
pyrrolic-like	3.5	8.89	1.40	5.84	2.88
	5.8	-1.94	-0.66	-1.42	0.55
	8.1	-0.94	-0.46	-0.74	0.31
	10.7	-0.18	-0.26	-0.27	0.23

and S4 in the Supporting Information, the energy barriers are negative for K^+ and Cl^- ions when hole diameter is greater than 4.2 Å, corresponding to a trapping state for an ion located at the hole center. For an elemental reaction, negative activation energy means that the reaction occurs without energy barrier and the reaction rate decreases with increasing temperature.^{53–55} For ion diffusion in supercapacitors, however, the ion has to climb out of the negative-energy trap in order to pass through the hole. Note that the hole attracts both cations and anions, because that the charging state of unsaturated bond of carbon has two possibilities: either as donor state to release nonbonding electron or as acceptor state to receive additional electron. However, the edge dangling bonds in the realistic graphene electrode are very likely saturated by functional groups in the aqueous solutions, which may affect the specific values of the penetration barriers for ions.

After doping with N atom as electron donor, the diffusion barriers of holes become more negative for K^+ ion and more positive for Cl^- ion simply due because of the electrostatic interaction (see Figures S5 and S6 in the Supporting Information). By comparison, the energy barriers of N-doped systems slightly overtop that of the undoped counterparts. This phenomenon can be explained in terms of the electronegativity (3.04 for N and 2.55 for C⁵⁶). Higher electronegativity means stronger chemical activity. Although the electrochemical processes are governed by a number of parameters, N-doped graphene as electrode is expected to exhibit enhanced capacitance because of the stronger binding energy for K^+ ion. As pointed out by Jeong et al.,¹⁵ stronger binding energy of potassium results in more ions accommodated on the electrode surface, which contribute to the increased capacitance.

The above results clearly indicate that charging state and bond saturation of carbon or nitrogen atoms on the hole periphery have significant influence on the ion transport behavior and capacitance of graphene electrodes. Our theoretical finding highlights the need for fine tuning size and bonding state of holes in porous electrode materials for supercapacitor applications.^{57–60} Experimentally, it was found that the amount of micropores plays a crucial role in ion

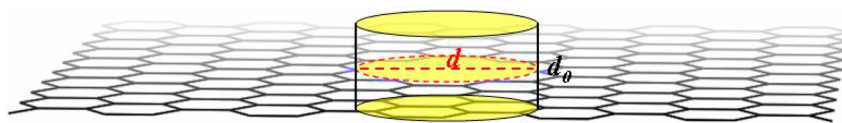


Figure 5. Schematic diagram of cylindrical pore on graphene sheet; d is hole diameter and $d_0 = 3.34 \text{ \AA}$ is the vdW distance between graphene layers.

Table 2. Intrinsic Strength (τ), and Critical Failure Strains (δ) for Different Systems

	N_V	$d (\text{\AA})$	Structure	Undoped		N doped	
				τ (GPa)	δ (%)	τ (GPa)	δ (%)
quaternary-like	0	0		114.7	25	114.5	23
triangular	1	2.8		99.3	16	88.7	13
triangular	9	5.5		55.2	10	57.2	9
rectangular	2	3.8		81.4	13	76.0	12
Hexagonal (rectangular)	6	6.4		68.3	11	70.1	13
pyrrolic-like	3	3.5		74.1	11	60.4	10
pyrrolic-like	12	5.8		52.4	10	50.7	10

accumulation in terms of ion adsorption behavior and these pores must be electrochemically accessible of ions.^{49,61}

The theoretical specific capacitance of supercapacitor¹⁴ can be calculated by

$$C = \epsilon \epsilon_0 A / l \quad (3)$$

where A is the effective specific surface area, l is the thickness of electric double layer, ϵ_0 is vacuum permittivity ($8.85 \times 10^{-12} \text{ F/m}$), and ϵ is relative dielectric constant of the electrolyte. For a given system, C is primarily determined by A while the other factors remain constants. To qualitatively estimate the capacitance of graphene electrode with holes or N dopants, in Figure 5 we built a structural model for the graphene sheet with cylindrical hole surface, where d is hole diameter and $d_0 = 3.34 \text{ \AA}$ is the vdW distance between graphene layers. After a hole is incorporated, the change of effective surface area can be approximated as

$$\Delta A = \pi d d_0 - \pi d^2 / 4 \quad (4)$$

where the first term is effect surface area of the hole edge that corresponds to a cylinder with height d_0 (see Figure 5), the second term is circular area of the hole. According to eq 4, as long as $d < 4d_0$ or $d < 13.36 \text{ \AA}$, the effective surface area increases ($\Delta A > 0$) and thus the capacitance is enhanced. When the hole edge atoms are further doped with N, the stronger binding between N and K^+/Cl^- ion would further increase the effective specific surface area, even though the geometry remains the same. In brief, graphene electrode with appropriate hole and N doping can enhance the specific capacitance.

In addition, because the realistic supercapacitors operate with electrolyte solution, the solvent effect is important. Since VASP is not able to simulate solvation effect, here we employed DMol³ program^{62,63} to consider the aqueous (H_2O) and organic (acetonitrile) electrolytes⁶⁴ using the so-called conductor-like screening model (COSMO).⁶⁵ Our test calculations of the diffusion behaviors of K^+ and Cl^- ions inside solvents (shown in the Table S1 in the Supporting Information) demonstrate that only the absolute values of the

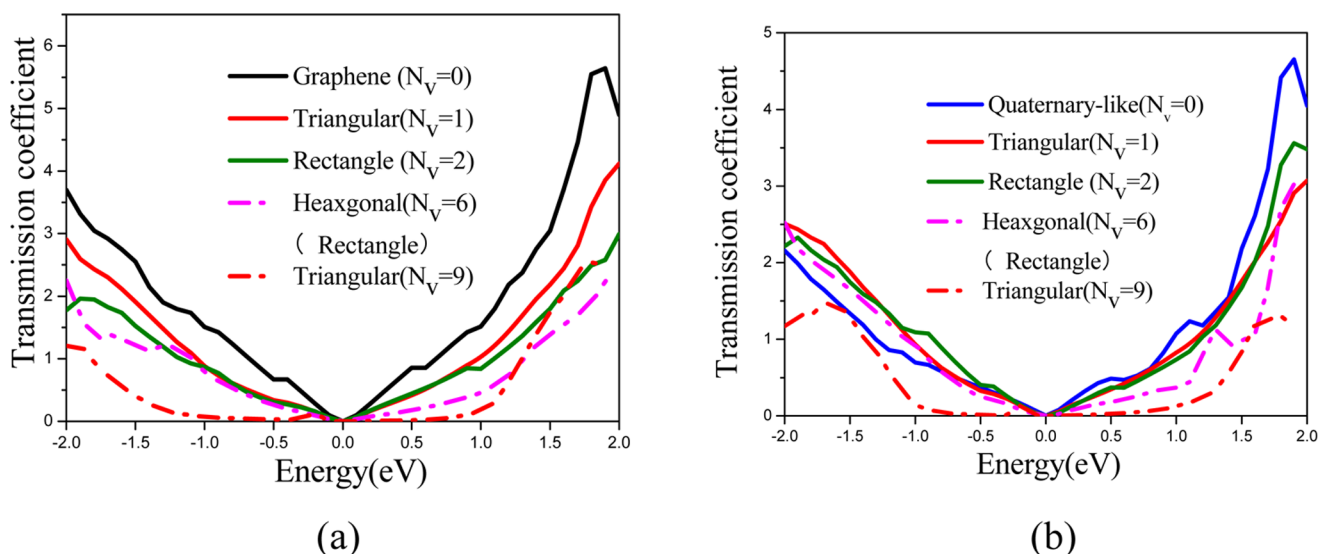


Figure 6. Transmission spectra of (a) graphene and (b) N-doped graphene with different hole shapes and sizes at zero bias voltage.

activation energy are systematically shifted by the choice of electrolyte solution, whereas the major conclusions such as the optimal hole size are not affected by solvent effect.

4.3. Intrinsic Strength. The stiffness and strength of the electrode material are the key factors of a supercapacitor for its long-term stability and fading of capacity upon cycling. Here we investigated the effects of holes shape or N-doping on the intrinsic mechanical properties of graphene sheets as electrode materials. Starting from the equilibrium supercell structures of N-doped and undoped graphene systems of the same dimension ($24.6 \text{ \AA} \times 17.06 \text{ \AA}$), one hole of various shapes and diameters (pyridinic-like: 2.8 and 5.5 \AA for triangular, 3.8 \AA for rectangular, 6.4 \AA for hexagonal or rectangular, corresponding to one, nine, two, and six vacancies, respectively; pyrrolic-like triangular: 3.5 and 5.8 \AA , corresponding to three and twelve vacancies, respectively) was introduced into the graphene sheet, as shown in Table 2. For a better comparison and to elucidate the role of N doping, we also considered quaternary-like system in which one N atom substitutes the C atom in the perfect graphene lattice.

Along the zigzag direction of graphene sheet, a series of uniaxial tensile strains were gradually applied with 1% increment, while the atomic coordinates were fully relaxed at each strain step. At given strain, the stress was computed directly for the simulation supercell using the stress theorem^{66,67} and then rescaled by a factor of Z/d_0 to obtain the equivalent stress on the graphene sheet, where $Z = 1.2 \text{ nm}$ is the thickness of vacuum space and $d_0 = 0.334 \text{ nm}$ stands for the van der Waals thickness of graphene layer.⁶⁸

Table 2 summarizes the calculated intrinsic strength (τ) and critical failure strains (δ) for different systems. The detailed theoretical stress-strain curves for every system are plotted in Figure S7 in the Supporting Information. For the perfect graphene sheet, our theoretical Young's modulus and intrinsic strength along the zigzag direction are $\sim 1 \text{ TPa}$ and 120 GPa , respectively, which coincide well with the experimental values (about 1 TPa and 130 GPa).⁶⁹

In the case of undoped graphene systems, the intrinsic strength generally reduces with increasing number of vacancies (i.e., hole size), which is roughly proportional to the number of broken C–C bonds and inversely proportional the energy

penalty to rupture the graphene sheet. The variation trend for intrinsic strengths from present first-principles calculations compare well with previous MD simulations.⁷⁰ In the range of the best hole diameters (4.2 – 10 \AA) for the different hole shapes, the system with pyridinic-like hexagonal hole has large effective aperture and still retains good intrinsic strength (about 70 GPa).

Substitutional doping with nitrogen keeps the mechanical strength of graphene sheet almost invariable and leads to only little reduction in the failure strain (by 2%), because that incorporation of N atoms in graphene lattice does not really interrupt π conjugate electrons. Comparing to the undoped systems with pyridinic-like hole defects, the intrinsic strengths of most N-doped graphene sheets with the same holes are smaller by $<10\%$. Meanwhile, the intrinsic strength of N doping with pyrrolic-like triangular hole of 3.5 \AA and 5.8 \AA diameters decrease by 18 and 3%, and the corresponding failure strains decrease by $<1\%$. In the range of optimal hole diameters (4.2 – 10 \AA), the N-doped system with pyridinic-like hexagonal hole not only preserves good intrinsic strength, but also possesses even better mechanical properties with regard to the undoped counterpart.

According to our theoretical analysis, the N-doped graphene sheets with pyridinic-like holes (especially hexagonal shape with hole diameter of 6.4 \AA) possess good permeability and retain the excellent mechanical properties of pristine graphene simultaneously, both of which are essential for the fast charge/discharge rate and long cycle life of electrode materials in supercapacitors. In experiment, Jeong et al. reported that the supercapacitors with nitrogen-doped graphene electrode possess high capacitance ($\sim 280 \text{ F/g}_{\text{electrode}}$) in which the pyridinic-like N dopant plays a major role and superior cycle life ($>200\,000$ cycles).¹⁵

4.4. Electronic and Transport Properties. Graphene with superior electrical conductivity is regarded as a good electrode material of supercapacitor.⁷¹ Characterization and understanding of the quantum transport properties of graphene electrodes are thus of fundamental importance for the practical applications of supercapacitor. Intuitively, the structural defects and nitrogen dopants in graphene sheet are expected to create higher density of active sites available for electron gain/loss on

the one hand; but break part of the intrastatal transport channels on the other hand. It is still unclear yet which effect plays a more dominant role in the transport properties for the N-doped graphene.

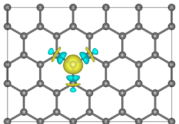
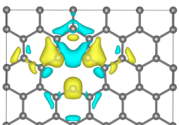
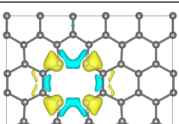
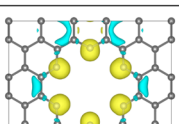
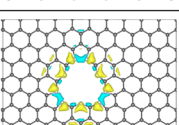
From the above theoretical results of the thermodynamic stabilities, mechanical properties and diffusion behaviors, N-doped graphene with pyridinic-like holes is in favor of serving as electrode material for supercapacitor. In experiments, it was shown that the specific doping type in N-doped graphene materials can be controlled by the catalyst preparation method.⁷² Therefore, in this subsection, we explore the effects of hole defect and N-dopant on the intrastatal transport properties of undoped and N-doped graphene sheets only with pyridinic-like holes using nonequilibrium Green's function. The following models in Table 2 were considered: (i) N-doped and undoped graphene systems with one pyridinic-like hole of various shapes and diameters (2.8 Å and 5.5 Å for triangular, 3.8 Å for rectangular, 6.4 Å for hexagonal/rectangular); (ii) quaternary-like system to distinguish the role of N dopants and hole defect.

Figure 6 presents the transmission spectra of undoped and N-doped graphene at zero bias voltage. When the number of vacancies is less than nine, all systems present zero transport gap like the pristine graphene,⁷³ implying that conduction electrons can transmit across the hole boundary perfectly. However, compared with the pristine graphene, their transmission coefficients are lower by about 19–68%. In other words, defects reduce the number of in-plane conduction channels and thus increase the resistivity. Such decline of electron transmission is more pronounced when the hole becomes bigger (i.e., with more vacancies). Beyond nine vacancies, there appears a defect-induced transport gap by about 2 eV, which would hinder electron conduction.

From Figure 6b, we can see that the transmission functions for the N-doped graphene systems with holes or without holes are comparable when the number of vacancies per hole is less than nine. Although the transmission coefficients of N-doped graphene sheets are still lower than that of pristine graphene, incorporation of nitrogen atoms seems to be able to prevent electron transport from further reducing, that is, the transmission spectra for N-doped graphene sheets with quaternary-like impurity ($N_v = 0$), and pyridinic-like holes of triangular ($N_v = 1$), rectangular ($N_v = 2$), hexagonal ($N_v = 6$) shapes are close to each other. We further analyzed the electronic properties of N-doped graphene in terms of N-induced redistributions of charge density (Table 3). One can see formation of strong C–N bonds and the electrons are mainly localized on nitrogen atoms. Both of which would induce electron conductivity similar to the Anderson localization effect.⁷⁴ The present theoretical results agree well with experiment,⁷⁵ in which N doped graphenes have lower conductivity with regard to pristine graphene. Most importantly, within the range of the optimal hole diameters (4.2–10 Å) of different shapes, the system with pyridinic-like hexagonal hole has preferable transmission characteristics which is crucial for the application of graphene electrode.

The above analysis of electronic properties shows that N-doping leads to accumulation of electrons on N atoms. This could generate high pseudocapacitance since N atom acts as electron donor to attract protons, in line with the results of ion diffusion where the N dopant exhibits the largest binding energy difference for potassium ion of the electrolyte compared to that of the pristine graphene.¹⁵ Experimentally, electrical measurements also demonstrate that the high capacitance of

Table 3. N-Induced Charge Redistribution Characterized by the Charge Density ($\rho_a - \rho_b$) Distributions with Different Hole Shapes for Pyridinic-Like and for Quaternary-Like System^a

	N_v	d (Å)	Structure
quaternary-like	0	0	
triangular	1	2.8	
rectangular	2	3.8	
Hexagonal (rectangular)	6	6.4	
triangular	9	5.5	

^aYellow and grey-blue represent the positive and negative charges, respectively. The isosurface value is set as ± 0.02 e/Å³.

144.6 F/g at 0.2 A/g for N-doped graphene might be the consequence of pyridinic nitrogen inducing electron donor properties to the layer.⁷⁶

5. CONCLUSIONS

To briefly summarize, here we theoretically exploited several critical issues of N-doped graphene sheets for their applications as electrode of supercapacitors. It was found that N-doped graphene with pyridinic-like hole are more thermodynamic stable and still retain their excellent mechanical properties, particularly for hexagonal holes. Moreover, the holes with average size from 4.2 to 10 Å allow the diffusive ions to penetration, resulting in increased capacitance. Although the transmission function for the N-doped graphene systems is lower than that of pristine graphene, they can retain a certain number of conduction channels from further reducing. Overall speaking, our first-principles results indicate that the N-doped graphene sheets with pyridinic-like hexagonal hole of optimal diameters (4.2–10 Å) stand out for reasonable thermodynamic stability, good intrinsic strength, and appreciable transmission spectrum. No doubt, the present theoretical findings will be important in guiding design of graphene-based materials as electrode for supercapacitor devices.

■ ASSOCIATED CONTENT

📄 Supporting Information

Illustration of the graphene-based devices for transport, formation energy of nitrogen doping, diffusion barriers for K⁺

and Cl^- ions, activation energies of K^+ and Cl^- ions with different solvent effect and stress-strain curves of undoped and N-doped graphene sheets are provided. This material is available free of charge via the Internet at <http://pubs.acs.org>.

AUTHOR INFORMATION

Corresponding Author

*Tel.: +86-411-84709748. E-mail address: zhaojj@dlut.edu.cn.

Notes

The authors declare no competing financial interest.

ACKNOWLEDGMENTS

This work was supported by the National Natural Science Foundation of China (11174242), the Natural Science Foundation of Jiangsu Province (BK2010499, BK2012255, BY2013064, BK20130458, BK20130431), CETV, and guoshi.com. L.L. acknowledges support through the Scholarship Award for Excellent Doctoral Student granted by the Ministry of Education of China.

REFERENCES

- (1) Simon, P.; Gogotsi, Y. *Nat. Mater.* **2008**, *7*, 845–854.
- (2) Qu, D. *J. Power Sources* **2002**, *109*, 403–411.
- (3) Xing, W.; Qiao, S.; Ding, R.; Li, F.; Lu, G.; Yan, Z.; Cheng, H. *Carbon* **2006**, *44*, 216–224.
- (4) Portet, C.; Yushin, G.; Gogotsi, Y. *Carbon* **2007**, *45*, 2511–2518.
- (5) Zhang, L. L.; Zhao, X. *Chem. Soc. Rev.* **2009**, *38*, 2520–2531.
- (6) Tang, Q.; Zhou, Z.; Chen, Z. *Nanoscale* **2013**, *5*, 4541–4583.
- (7) Zhang, L. L.; Zhou, R.; Zhao, X. *J. Mater. Chem.* **2010**, *20*, 5983–5992.
- (8) Cheng, Q.; Tang, J.; Shiny, N.; Qin, L. *J. Power Sources* **2013**, *241*, 423–428.
- (9) Suk, J. W.; Piner, R. D.; An, J.; Ruoff, R. S. *ACS Nano* **2010**, *4*, 6557–6564.
- (10) Liu, L.; Zhang, J.; Zhao, J.; Liu, F. *Nanoscale* **2012**, *4*, 5910–5916.
- (11) Stoller, M. D.; Park, S.; Zhu, Y.; An, J.; Ruoff, R. S. *Nano Lett.* **2008**, *8*, 3498–3502.
- (12) Wang, X.; Li, X.; Zhang, L.; Yoon, Y.; Weber, P. K.; Wang, H.; Guo, J.; Dai, H. *Science* **2009**, *324*, 768–771.
- (13) Zhu, Y.; Murali, S.; Stoller, M. D.; Ganesh, K.; Cai, W.; Ferreira, P. J.; Pirkle, A.; Wallace, R. M.; Cychosz, K. A.; Thommes, M. *Science* **2011**, *332*, 1537–1541.
- (14) Zhang, L.; Yang, X.; Zhang, F.; Long, G.; Zhang, T.; Leng, K.; Zhang, Y.; Huang, Y.; Ma, Y.; Zhang, M. *J. Am. Chem. Soc.* **2013**, *135*, 5921–5929.
- (15) Jeong, H. M.; Lee, J. W.; Shin, W. H.; Choi, Y. J.; Shin, H. J.; Kang, J. K.; Choi, J. W. *Nano Lett.* **2011**, *11*, 2472–2477.
- (16) Qiu, Y.; Zhang, X.; Yang, S. *Phys. Chem. Chem. Phys.* **2011**, *13*, 12554–12558.
- (17) Shao, Y.; Zhang, S.; Engelhard, M. H.; Li, G.; Shao, G.; Wang, Y.; Liu, J.; Aksay, I. A.; Lin, Y. *J. Mater. Chem.* **2010**, *20*, 7491–7496.
- (18) Hassan, F. M.; Chabot, V.; Li, J.; Kim, B. K.; Ricardez-Sandoval, L.; Yu, A. *J. Mater. Chem. A* **2013**, *1*, 2904–2912.
- (19) Sun, L.; Wang, L.; Tian, C.; Tan, T.; Xie, Y.; Shi, K.; Li, M.; Fu, H. *RSC Adv.* **2012**, *2*, 4498–4506.
- (20) Jin, Z.; Yao, J.; Kittrell, C.; Tour, J. M. *ACS Nano* **2011**, *5*, 4112–4117.
- (21) Panchakarla, L.; Subrahmanyam, K.; Saha, S.; Govindaraj, A.; Krishnamurthy, H.; Waghmare, U.; Rao, C. *Adv. Mater.* **2009**, *21*, 4726–4730.
- (22) Li, X.; Wang, H.; Robinson, J. T.; Sanchez, H.; Diankov, G.; Dai, H. *J. Am. Chem. Soc.* **2009**, *131*, 15939–15944.
- (23) Wei, L.; Sevilla, M.; Fuertes, A. B.; Mokaya, R.; Yushin, G. *Adv. Energy Mater.* **2011**, *1*, 356–361.
- (24) Mukherjee, S.; Kaloni, T. *J. Nanopart. Res.* **2012**, *14*, 1–5.
- (25) Jalili, S.; Vaziri, R. *Mol. Phys.* **2011**, *109*, 687–694.
- (26) Deifallah, M.; McMillan, P. F.; Cora, F. *J. Phys. Chem. C* **2008**, *112*, 5447–5453.
- (27) Cervantes-Sodi, F.; Csanyi, G.; Piscanec, S.; Ferrari, A. *Phys. Rev. B* **2008**, *77*, 165427(1–13).
- (28) Li, Y.; Zhou, Z.; Shen, P.; Chen, Z. *ACS Nano* **2009**, *3*, 1952–1958.
- (29) Yan, H.; Xu, B.; Shi, S.; Ouyang, C. *J. Appl. Phys.* **2012**, *112*, 104316(1–5).
- (30) Wu, D.; Li, Y.; Zhou, Z. *Theor. Chem. Acc.* **2011**, *130*, 209–213.
- (31) Ma, C.; Shao, X.; Cao, D. *J. Mater. Chem.* **2012**, *22*, 8911–8915.
- (32) Golberg, D.; Bando, Y.; Huang, Y.; Terao, T.; Mitome, M.; Tang, C.; Zhi, C. *ACS Nano* **2010**, *4*, 2979–2993.
- (33) Kresse, G.; Furthmüller, J. *Comput. Mater. Sci.* **1996**, *6*, 15–50.
- (34) Blöchl, P. E. *Phys. Rev. B* **1994**, *50*, 17953–17979.
- (35) Kresse, G.; Hafner, J. *Phys. Rev. B* **1993**, *47*, 558–561.
- (36) Perdew, J. P.; Burke, K.; Ernzerhof, M. *Phys. Rev. Lett.* **1996**, *77*, 3865–3868.
- (37) Lee, H. Y.; Goodenough, J. B. *J. Solid State Chem.* **1999**, *144*, 220–223.
- (38) Reddy, R. N.; Reddy, R. G. *J. Power Sources* **2006**, *156*, 700–704.
- (39) Henkelman, G.; Arnaldsson, A.; Jónsson, H. *Comput. Mater. Sci.* **2006**, *36*, 354–360.
- (40) Henkelman, G.; Uberuaga, B. P.; Jónsson, H. *J. Chem. Phys.* **2000**, *113*, 9901–9904.
- (41) Taylor, J.; Guo, H.; Wang, J. *Phys. Rev. B* **2001**, *63*, 245407(1–13).
- (42) Wang, J.; Guo, H. *Phys. Rev. B* **2009**, *79*, 045119(1–5).
- (43) Koskinen, P.; Malola, S.; Häkkinen, H. *Phys. Rev. Lett.* **2008**, *101*, 115502(1–4).
- (44) Gao, J.; Zhao, J.; Ding, F. *J. Am. Chem. Soc.* **2012**, *134*, 6204–6209.
- (45) Wassmann, T.; Seitsonen, A. P.; Saitta, A. M.; Lazzeri, M.; Mauri, F. *Phys. Rev. Lett.* **2008**, *101*, 96402(1–4).
- (46) Guo, B.; Liu, Q.; Chen, E.; Zhu, H.; Fang, L.; Gong, J. R. *Nano Lett.* **2010**, *10*, 4975–4980.
- (47) Bruce, P. G.; Hardwick, L. J.; Abraham, K. *MRS Bull.* **2011**, *36*, 506–512.
- (48) Raymundo-Pinero, E.; Kierzek, K.; Machnikowski, J.; Beguin, F. *Carbon* **2006**, *44*, 2498–2507.
- (49) Chmiola, J.; Yushin, G.; Gogotsi, Y.; Portet, C.; Simon, P.; Taberna, P. L. *Science* **2006**, *313*, 1760–1763.
- (50) Vineyard, G. H. *J. Phys. Chem. Solids* **1957**, *3*, 121–127.
- (51) Shannon, R. *Acta Crystallogr. Sect. A* **1976**, *32*, 751–767.
- (52) Salitra, G.; Soffer, A.; Eliad, L.; Cohen, Y.; Aurbach, D. *J. Electrochem. Soc.* **2000**, *147*, 2486–2493.
- (53) Alvarez-Idaboy, J. R.; Mora-Diez, N.; Vivier-Bunge, A. *J. Am. Chem. Soc.* **2000**, *122*, 3715–3720.
- (54) Villà, J.; González-Lafont, A.; Lluch, J. M.; Corchado, J. C.; Espinosa-García, J. *J. Chem. Phys.* **1997**, *107*, 7266–7274.
- (55) Cunningham, D.; Vogel, W.; Haruta, M. *Catal. Lett.* **1999**, *63*, 43–47.
- (56) Xiao, J.; Staniszewski, J.; Gillespie, J. *Mater. Sci. Eng., A* **2010**, *527*, 715–723.
- (57) Zhang, L.; Zhang, F.; Yang, X.; Long, G.; Wu, Y.; Zhang, T.; Leng, K.; Huang, Y.; Ma, Y.; Yu, A. C.; Yongsheng, S. *Sci. Rep.* **2013**, *3*, 01408(1–9).
- (58) Richey, F. W.; Dyatkin, B.; Gogotsi, Y.; Elabd, Y. A. *J. Am. Chem. Soc.* **2013**, *135*, 12818–12826.
- (59) Chen, Z.; Wen, J.; Yan, C.; Rice, L.; Sohn, H.; Shen, M.; Cai, M.; Dunn, B.; Lu, Y. *Adv. Energy Mater.* **2011**, *1*, 551–556.
- (60) Fan, Z.; Liu, Y.; Yan, J.; Ning, G.; Wang, Q.; Wei, T.; Zhi, L.; Wei, F. *Adv. Energy Mater.* **2012**, *2*, 419–424.
- (61) Wang, D. W.; Li, F.; Liu, M.; Lu, G. Q.; Cheng, H. M. *Angew. Chem.* **2008**, *120*, 379–382.
- (62) Delley, B. *J. Chem. Phys.* **1990**, *92*, 508–517.
- (63) Delley, B. *J. Chem. Phys.* **2000**, *113*, 7756–7764.
- (64) Simon, P.; Gogotsi, Y. *Acc. Chem. Res.* **2012**, *46*, 1094–1103.
- (65) Klamt, A.; Schüürmann, G. *J. Chem. Soc.* **1993**, *2*, 799–805.

- (66) Nielsen, O.; Martin, R. M. *Phys. Rev. Lett* **1983**, *50*, 697–700.
- (67) Nielsen, O.; Martin, R. M. *Phys. Rev. B* **1985**, *32*, 3780–3791.
- (68) Zhang, J.; Zhao, J.; Lu, J. *ACS Nano* **2012**, *6*, 2704–2711.
- (69) Lee, C.; Wei, X.; Kysar, J. W.; Hone, J. *Science* **2008**, *321*, 385–388.
- (70) Ito, A.; Okamoto, S. *IMECS* **2012**, *1*, 320–325.
- (71) Stankovich, S.; Dikin, D. A.; Piner, R. D.; Kohlhaas, K. A.; Kleinhammes, A.; Jia, Y.; Wu, Y.; Nguyen, S. B. T.; Ruoff, R. S. *Carbon* **2007**, *45*, 1558–1565.
- (72) Niwa, H.; Horiba, K.; Harada, Y.; Oshima, M.; Ikeda, T.; Terakura, K.; Ozaki, J.-i.; Miyata, S. *J. Power Sources* **2009**, *187*, 93–97.
- (73) Scrosati, B. *J. Electrochem. Soc.* **1992**, *139*, 2776–2781.
- (74) Xiong, S. J.; Xiong, Y. *Phys. Rev. B* **2007**, *76*, 214204(1-10).
- (75) Ortiz Medina, J.; García Betancourt, M. L.; Jia, X.; Martínez Gordillo, R.; Pelagio Flores, M. A.; Swanson, D.; Elías, A. L.; Gutiérrez, H. R.; Gracia Espino, E.; Meunier, V. *Adv. Funct. Mater.* **2013**, *23*, 3755–3762.
- (76) Jiang, B.; Tian, C.; Wang, L.; Sun, L.; Chen, C.; Nong, X.; Qiao, Y.; Fu, H. *Appl. Surf. Sci.* **2012**, *258*, 3438–3443.